Supporting information for

Rubidium Ion Capture with a Phosphotungstic Acid Functionalized Finger-Citron-Residue-Based Carbon

Qing Liu[a], Guihua Zhao[a], Yifang Dai[b], Na Ma[c] and Wei Dai [a],*

[a] *College of Chemistry and Life Science, Zhejiang Normal University, Zhejiang Province, Jinhua 321004, PR China*

[b] *Class 14 of first Grade, Jinhua No.1 High School, Zhejiang Province, Jinhua 321004, PR China*

[c] *College of Geography and Environmental Sciences, Zhejiang Normal University, Zhejiang Province, Jinhua 321004, PR China*

Section 1:

The Brunauer−Emmett−Teller (BET) surface areas and pore size distributions of the adsorbents were determined by multipoint N_2 adsorption−desorption at liquid N_2 temperature (−196 °C) on a physical adsorption instrument (Micromeritics, ASAP2020). Prior to analysis, all samples were subjected to a vacuum at 200 °C to ensure a clean surface. The specific surface areas were calculated using the standard Brunauer-Emmett-Teller (BET) method, which is the most widely used model for determining the specific surface area. The surface area of the samples was calculated from the nitrogen adsorption isotherms by assuming the area of a nitrogen molecule to be 0.162 nm^2. The micropore volumes was obtained from the *t*-plot method. The total pore volumes were estimated to be the liquid volumes of N_2 at a relative pressure of 0.99. The pore size distribution and average pore diameter were calculated using the nonlocal density functional theory (NLDFT) model. X-ray powder diffraction patterns

were recorded on a Philips PW 1710 diffractometer with automatic control. The patterns were obtained with monochromatic Cu Kα radiation with a scan rate of 2 $^{o}C\cdot min^{-1}$. Fourier transform infrared (IR) spectra were recorded on a Nicolet Nexus 470 spectrometer with KBr wafer. The contact angle of as-prepared adsorbents was measured using a Dataphysics OCA20 contact angle system in ambient air at room temperature. The scanning electron microscopy (SEM) images were determined by an electron microscope (Hitachi S4800).

Section 2:

Figure S.I. captions:

Fig. S.I.1. Pore size distributions of PTA@FMC materials.

Fig. S.I.2. SEM images of PTA@FMC materials, in which (a), (b) represent the SEM images of FMC and (c), (d) represent the SEM images of PTA@FMC.

Fig. S.I.3. Fourier infrared rays of PTA@FMC materials.

Fig. S.I.4. XRD patterns of PTA@FMC materials at cornule.

Fig. S.I.5. Influence of the number of interfering ions on the adsorption capacity of Rb^+ onto FMC and PTA@FMC.

Fig. S.I.6. The reduction rate of the adsorption amount of Rb^+ and the number of interfering ions.

Fig. S.I.7 Effect of recycle times of FPC-1 on the CR adsorption capacity.
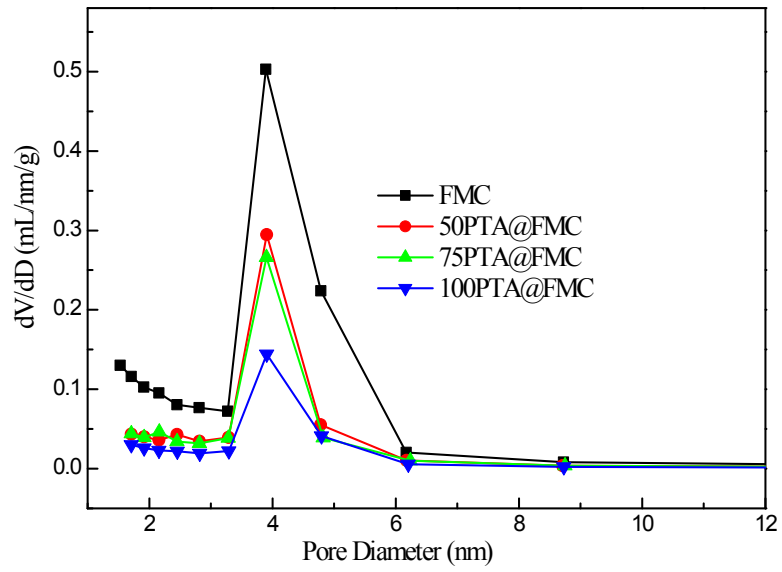
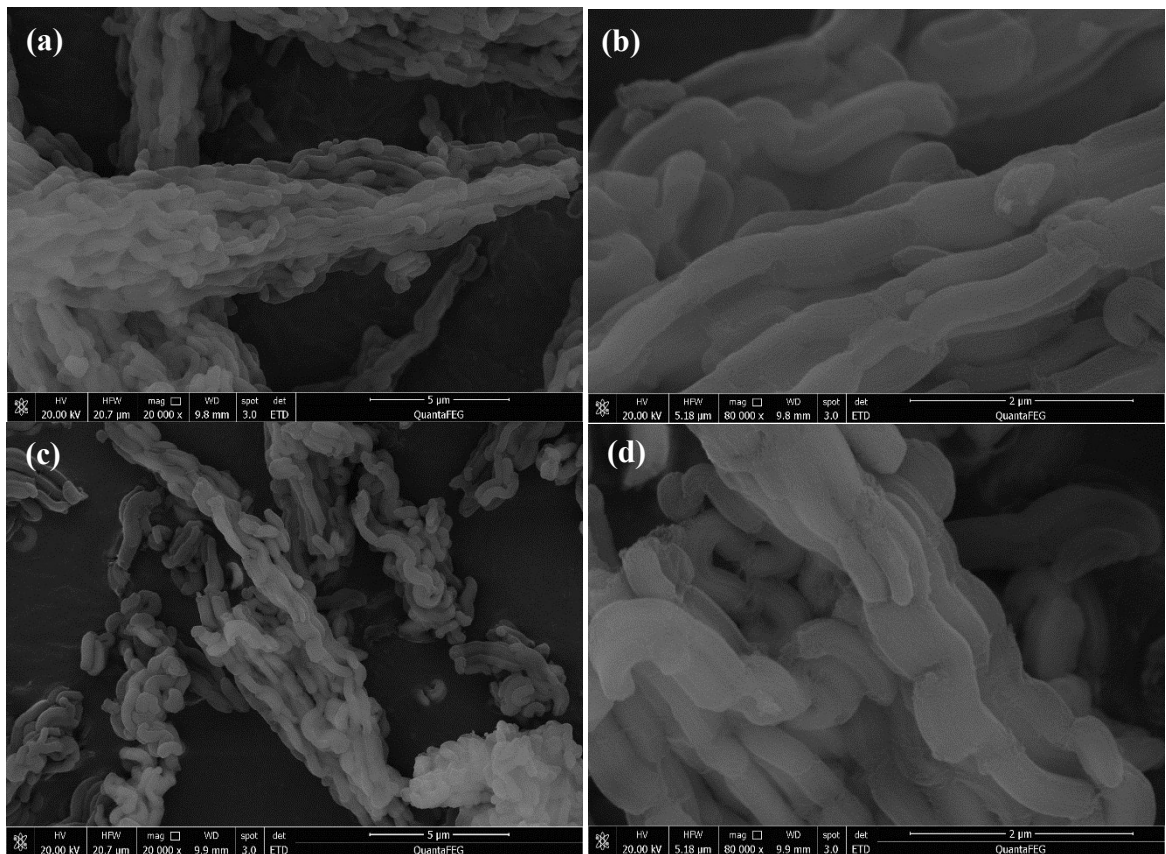**Fig. S.I.1.** Pore size distributions of PTA@FMC materials.

Fig. S.I.2. SEM images of PTA@FMC materials, in which (a), (b) represent the SEM images of FMC and (c), (d) represent the SEM images of PTA@FMC.
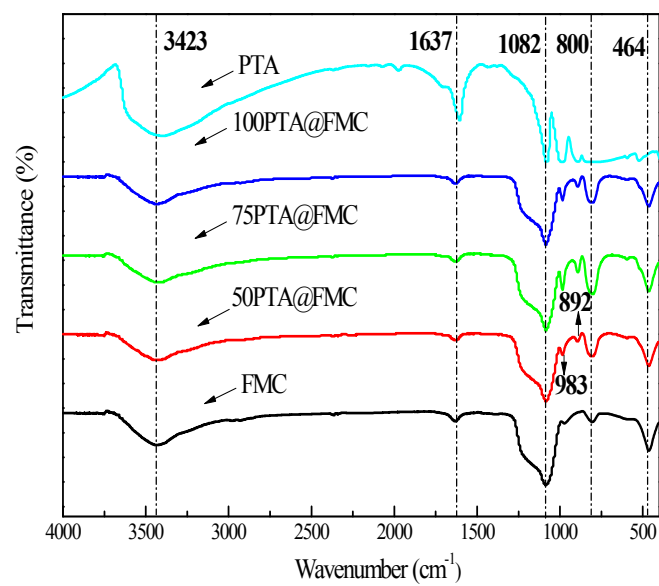
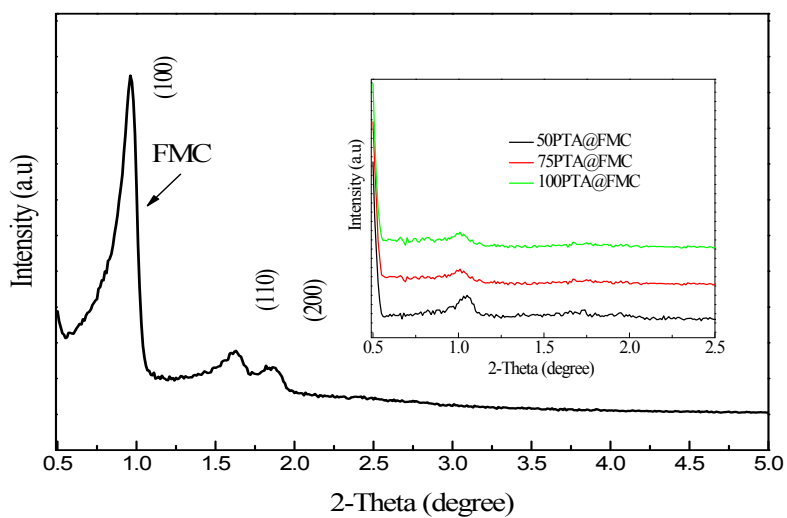**Fig. S.I.3.** Fourier infrared rays of PTA@FMC materials.

Fig. S.I.4. XRD patterns of PTA@FMC materials at cornule.
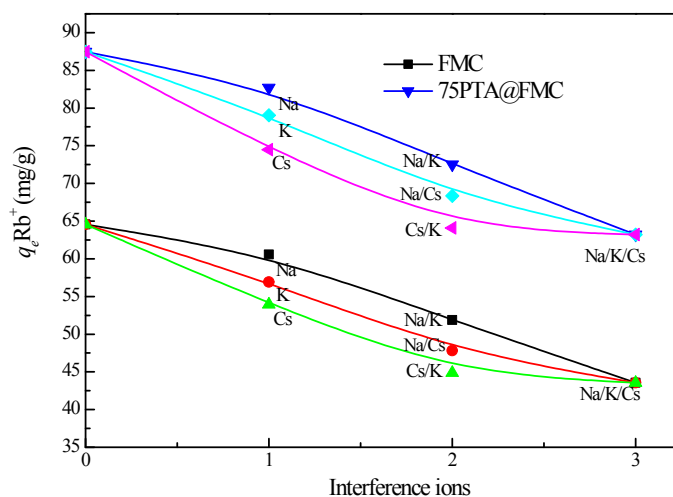
Fig. S.I.5. Influence of the number of interfering ions on the adsorption capacity of Rb$^+$ onto FMC and PTA@FMC.
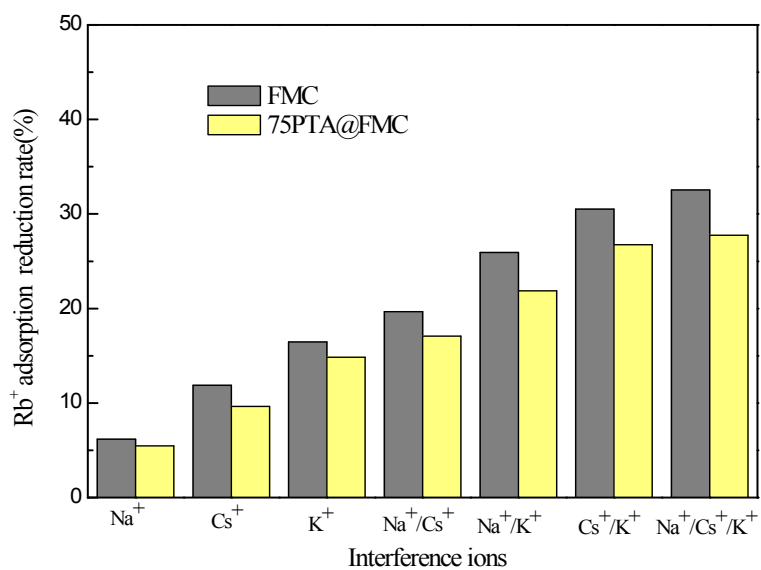

Fig. S.I.6. The reduction rate of the adsorption amount of Rb$^+$ and the number of interfering ions.
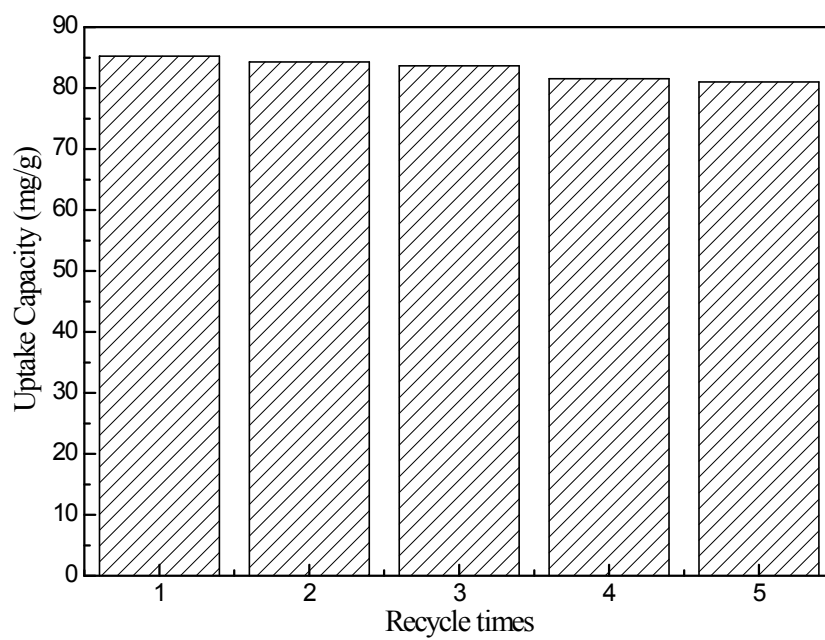
Fig. S.I.7 Effect of recycle times of FPC-1 on the CR adsorption capacity.

Section 3:

Table S.I. captions:

Table S.I.1. Structural properties of FMC, 50PTA@FMC, 75PTA@FMC and 100PTA@FMC, respectively

Table S.I.2. Comparison of the maximum uptake capacities of Rb^+ on various adsorbents. (C_0=100mg/L, pH=7, T=25°C)

Table S.I.3 Different isotherm models and their linear forms

Table S.I.4. Parameters of the isotherm models for the adsorption processes

Table S.I.5 Calculation equations

Table S.I.6. Parameters of the adsorption kinetics for the adsorption processes

Table S.I.1. Structural properties of FMC, 50PTA@FMC, 75PTA@FMC and 100PTA@FMC, respectively

Materials	$S_{BET}(m^2/g)$	$V(cm^3/g)$	Pore width(nm)
FMC	628.54	0.97	6.565
50PTA@FMC	284.32	0.48	6.550
75PTA@FMC	263.36	0.45	6.548
100PTA@FMC	176.42	0.25	6.549

Table S.I.2. Comparison of the maximum uptake capacities of Rb^+ on various adsorbents. (C_0=100mg/L, pH=7, T=25°C)

Metal ion	Adsorbent	Maximum uptake capacities (mg/g)	Reference
Rb	FMC	66.65	this work
	75PTA@FMC	86.50	this work
	MIL-101(Cr)	72.88	this work
	Co-PBA	20	[3]
	KCoFC(L)	70	[23]
	KCuFC(PAN)	7.85	[23]
	Calcium Alginate	20.64	[24]
	MBI-Imogolite	26.11	[23]
	K(Cu)FC	86.32	[23]
	Mordenite	14.50	[23]

Table S.I.3 Different isotherm models and their linear forms

Isotherm	Nonlinear form	Linear form	Plot	Eqs.
Langmuir-I	$q_e = \dfrac{K_L C_e}{1 + K_L C_e}$	$\dfrac{C_e}{q_e} = \dfrac{1}{q_L \cdot K_L} + \left(\dfrac{1}{q_L}\right) \cdot C_e$	$\dfrac{C_e}{q_e}$ versus C_e	(1)
Freundlich	$q_e = K_f C_e^{\frac{1}{n}}$	$\ln q_e = \ln K_f + \left(\dfrac{1}{n}\right) \cdot \ln C_e$	$\ln q_e$ versus $\ln C_e$	(2)
Temkin	$q_e = K_t^{\beta} C_e$	$\ln q_e = \beta \ln K_t + \ln C_e$	$\ln q_e$ versus $\ln C_e$	(3)
D-R	$q_e = q_s e^{(-K_D \varepsilon^2)}$	$\ln q_e = \ln q_s - K_D \varepsilon^2$	$\ln q_e$ versus ε^2	(4)

Where q_e is the equilibrium adsorption capacity in mg/g; K_L is a constant related to the affinity of the binding sites in L/mg; 'K_f' and 'n' are measures of adsorption capacity and the intensity of adsorption respectively; $\beta = (RT)/bT$, is the Temkin constant; T is the absolute temperature in K; R is the universal gas constant; qs is the D-R isotherm constant in mg/g; and ε represents the Polanyi potential constant in kJ mol-1;

Table S.I.4. Parameters of the isotherm models for the adsorption processes

Samples	Langmuir			Freundlich			Temkin			D-R		
	q_m (mg/g)	K_L (L/mg)	R^2	K_f (L/g)	n	R^2	b_T (kJ/mol)	K_T (L/g)	R^2	q_s (mg/g)	K_D (mol²/kJ²)	R^2
0	67.57	3.177E-05	0.1424	0.9350	0.996	0.9977	86.38	0.1241	0.8853	41.46	2.253E-05	0.7002
50	79.76	8.347E-06	0.1250	1.2414	1.003	0.9960	72.79	0.1362	0.8843	51.17	1.95E-05	0.7204
75	87.48	7.824E-04	0.8657	2.6871	1.184	0.9925	73.49	0.1868	0.9228	58.62	1.308E-05	0.7521
100	76.79	5.401E-04	0.0418	1.2241	1.016	0.9969	76.69	0.1354	0.8872	49.30	2.030E-05	0.7313

Table S.I.5 Calculation equations

Name	equations	Eqs.
Pseudo-first order model	$\ln(q_e - q_t) = \ln(q_e) - K_1 t$	(4)
Pseudo-second order model	$\dfrac{t}{q_t} = \dfrac{1}{K_2 q_e} + \dfrac{t}{q_e}$	(5)
Intra-particle diffusion model	$q_t = K_3 t^{1/2}$	(6)

Where q_e and q_t (mg/g) are the uptakes of thiophene at equilibrium and at time t (min), respectively, K_1 (1/min) is the adsorption rate constant, K_2 (g/mg.min) is the rate constant for the second-order equation, and K_3 (mg/g.min$^{1/2}$) is the intra-particle diffusion rate constant.

Table S.I.6. Parameters of the adsorption kinetics for the adsorption processes

Sample	Ion	$q_{e,exp}$ (mg/g)	Pseudo-first-order rate equation					Pseudo-second-order rate equation					Intra-particle diffusion model		
			$q_{e,cal}$ (mg/g)	K_1 (1/min)	R^2	Δq(mg/g)	Δq(%)	$q_{e,cal}$ (mg/g)	K_2 (g/mgmin)	R^2	Δq(mg/g)	Δq(%)	C (mg/g)	K_3 (mg/g min$^{1/2}$)	R^2
FMC		67.57	3.0882	-0.0048	0.2454	64.48	95.30	67.57	0.1506	0.9995	0.81	1.05	62.54	0.7060	0.0569
50		79.76	4.7715	-0.02404	0.0093	74.99	94.18	79.76	0.0467	0.9996	1.51	1.97	66.93	1.8565	0.3012
75	Rb$^+$	87.48	6.7831	-0.03638	0.1632	80.70	92.46	87.48	0.0230	0.9997	0.52	0.98	71.88	2.3079	0.4555
100		76.79	4.1167	-0.06731	0.4220	72.67	94.39	76.79	0.0323	0.9999	0.43	0.56	67.48	1.4570	0.5507